

Development of Microstrip Structure and Microstrip Sensor for Measurement of Transient Electromagnetic Pulse

Jinhong Wei, Shoulong Zhang, Zhen Liu, Youjie Yan, Tingyong Jiang, and Fanghong Huang

Northwest Institute of Nuclear Technology
Xi'an 710049, China
17600809313@163.com

Abstract — In this paper, a type of microstrip structure and sensor based on the microstrip structure are designed, fabricated and tested for the measurement of transient electromagnetic pulse. The voltage on the terminal load of microstrip line illuminated by a plane wave is analyzed, and a method of recovering the incident electric field is presented to recover the transient electromagnetic pulse by numerical processing. The proposed microstrip structures are set on the shielding boxes. The start of microstrip structure 1 without substrate is short circuited, and the start of microstrip structure 2 with substrate is matched. The induced voltage is acquired from the ends of microstrip structures. The simulated results and the measured results verify that the microstrip structures can be used to measure the transient electromagnetic pulse with rise time of ≥ 1 ns. The simulated results show that the microstrip structures have wide bandwidths of 1.5 GHz and 2.5 GHz, respectively. In addition, the simulated effective heights show consistency with the measured effective heights. The microstrip sensors, built by adding the electro-optical conversion modules into the shielding boxes, have good fidelity and can be used to measure high-altitude electromagnetic pulse (HEMP).

Index Terms — Effective height, HEMP, microstrip structure, sensor, transient electromagnetic pulse.

I. INTRODUCTION

Transient electromagnetic pulse (EMP) [1] has the fast rise time and high amplitude. It is easy to be coupled into the internal electronic system, and can disrupt or damage critical electronic facilities over a very large area. HEMP and ultra-wideband short pulse (UWB-SP) are two kinds of typical transient electromagnetic pulses [2-5]. In order to reveal the characteristics of transient electromagnetic fields, clarify the effect of electromagnetic pulse on the electronic equipment, evaluate the performance of electromagnetic protection, and then seek for some important means of electromagnetic protection. The time domain measurement theory and technologies of transient electromagnetic field have

become one of the focal points in the region of EMP attack and protection.

The key technology in transient electromagnetic field measurement is to transform pulse field into voltage or current signal undistorted. The capabilities of the receiving antenna directly affect the test system to measure the pulsed field. TEM horn is used as the receiving antenna for UWB-SP recommended by NIST (National Institute of Standards and Technology) [6]. Within the time window of TEM horn, its output voltage waveform is identical to the incident electric field. The effective height of TEM horn is incalculable analytically and has to be calibrated by standard field or multi antenna method. When used in a narrow space, TEM horn may be too large to ignore the disturbance caused by the receiving antenna. The rise time of HEMP defined by IEC standard 61000-2-9 is 2.5 ± 0.5 ns, the pulsewidth is 23 ± 5 ns [7]. E-field sensor, D-Dot are the most commonly used electric field sensor for HEMP measurement [8-9]. Currently, the active E-field sensors based on the electrically small antenna need the matching networks of high impedances. The narrow frequency band of the networks becomes the limitation of the whole measurement systems [10]. The output of a D-dot sensor is proportional to the time rate of change of the measured field, and an integration operation has to be applied so as to restore the pulse shape of the electric field. In addition, the connection with balun, integral module, and electro-optical converting module further increases the overall size of the system.

VNIIOFI (All-Russian Research Institute for Optical and Physical Measurements) suggested using microstrip lines for measurement of EMP waveform parameters [11]. They developed the theory of microstrip transducers (IPPL-L) [12], carried out the experimental investigations and worked out the production technology [13-14]. One advantages of transducers is the flat transient response during the time window that is twice the time taken for the signal to propagate along the microstrip line. The output signals of the transducers replicate the E-field signal and any integration device is not necessary. Therefore, microstrip transducers are

optimal to record the UWB-SP. However, for the measurement of HEMP, since the duration time of the pulse waveforms are up to 100 ns or even more, the transducers lack a long enough time window to restore the incident waveform.

In this paper, two novel microstrip structures and microstrip sensors are proposed. The sensors adopt microstrip structures as the receiving antennas. The incident electric field can be recovered from the output signal recorded by the receiving antenna by the method of numerical processing. With the characteristics of wide bandwidth, good fidelity and compact sizes, they can be used to measure transient electromagnetic pulse.

II. STRUCTURE DESIGN

A. Microstrip line coupling to electromagnetic wave

Consider a microstrip line consisting of a conductor of length l and a ground plane parallel to the conductor, which are separated by a dielectric plate with the thickness h and the relative dielectric permittivity ϵ_r . Both of ends are loaded with impedances Z_1 and Z_2 respectively. The microstrip line is illuminated by a linearly polarized uniform plane wave as seen in Fig. 1.

Assume that $w \ll a$, $h \ll l$, and $h \ll a$, since the vector E of the incident field is perpendicular to the microstrip line carrier, it lies in the incidence plane, which corresponds to the case of vertical or parallel polarization. Thereby, the Poynting's P is parallel to the carrier plane. The voltage on the load Z_2 induced by the plane wave is representable in the form:

$$u(l,t) = \frac{E_0 h (1 + \rho_2)}{2} \sum_{k=0}^{\infty} (\rho_1 \rho_2)^k \cdot \left\{ \left[\frac{1 - \frac{1}{\epsilon_r}}{\sqrt{\epsilon_e} - 1} - \frac{1}{\epsilon_r} \right] \cdot \left[f\left(t - \frac{2lk\sqrt{\epsilon_e} + l}{c}\right) - f\left(t - \frac{(2k+1)l\sqrt{\epsilon_e}}{c}\right) \right] - \right. \quad (1)$$

$$\left. \rho_1 \left[\frac{1 - \frac{1}{\epsilon_r}}{\sqrt{\epsilon_e} + 1} + \frac{1}{\epsilon_r} \right] \cdot \left[f\left(t - \frac{(2k+1)l\sqrt{\epsilon_e}}{c}\right) - f\left(t - \frac{2l(k+1)\sqrt{\epsilon_e} + l}{c}\right) \right] \right\}$$

where E_0 is an external field strength of the incidence wave outside the dielectric substrate, f is the function determining a pulse waveform. c denotes light speed, ϵ_e is the equivalent dielectric constant of microstrip line. ρ_1 and ρ_2 are the reflection coefficients at both ends of the microstrip line,

$$\rho_1 = \frac{Z_1 - Z_c}{Z_c + Z_1}, \quad \rho_2 = \frac{Z_2 - Z_c}{Z_c + Z_2}. \quad (2)$$

Ignore the transmission loss of the current signal on the microstrip line. When $Z_1=0$, $Z_2=Z_c$, thus $\rho_1=-1$, $\rho_2=0$, analyzing (1) for the case of the dielectric layer being absent, and the induced voltage on the terminal load Z_2 can be expressed as:

$$U_{without_sub} = -\frac{E_0 h}{2} \left[f\left(t - \frac{l}{c}\right) - f\left(t - \frac{3l}{c}\right) \right]. \quad (3)$$

When $Z_1=Z_c$, $Z_2=Z_c$, thus $\rho_1=0$, $\rho_2=0$, analyzing (1) for the case of the dielectric layer being present, the induced voltage on the terminal load Z_2 can be written as:

$$U_{with_sub} = \frac{E_0 h}{2} \left[\frac{1 - \frac{1}{\epsilon_r}}{\sqrt{\epsilon_e} - 1} - \frac{1}{\epsilon_r} \right] \cdot \left[f\left(t - \frac{l\sqrt{\epsilon_e}}{c}\right) - f\left(t - \frac{l}{c}\right) \right]. \quad (4)$$

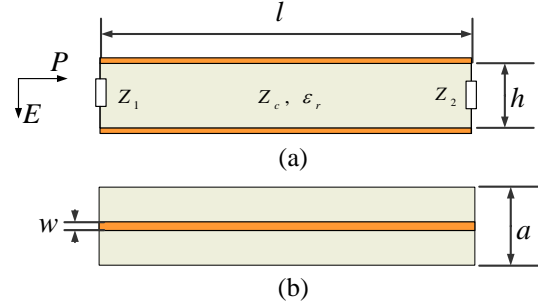


Fig. 1. Microstrip line illuminated by a plane wave: (a) side view and (b) top view.

B. The method of recovering the incident electric field

Based on (3) and (4) that the voltage signals can be expressed as the superposition of two voltage signals. If the two voltage signals are expressed as $V(t)$ and $-V(t-t_0)$ respectively, where t_0 expressed as the delay time, (3) and (4) can be representable in the form:

$$U(t) = V(t) - V(t - t_0). \quad (5)$$

Further, we can get,

$$V(t) = \sum_{n=0}^k U(t - nt_0) + V(t - (k+1)t_0). \quad (6)$$

When $(k+1)t_0$ is longer than the duration of the voltage signal $V(t)$, $V(t - (k+1)t_0)$ is after $V(t)$, the $V(t)$ can be get from the equation:

$$V(t) = \sum_{n=0}^k U(t - nt_0), \quad t < (k+1)t_0. \quad (7)$$

Combining Equations (3) and (4), we can get:

$$\sum_{n=0}^k U_{without_sub}\left(t - \frac{2nl}{c}\right) = -\frac{h}{2} E_0 f\left(t - \frac{l}{c}\right) \\ = -h_{eff1} E_0 f\left(t - \frac{l}{c}\right), \quad t < (k+1) \frac{2l}{c}, \quad (8)$$

$$\sum_{n=0}^k U_{with_sub}\left(t - n \frac{l\sqrt{\epsilon_e} - l}{c}\right) = \frac{h}{2} \left(\frac{1 - \frac{1}{\epsilon_r}}{\sqrt{\epsilon_e} - 1} - \frac{1}{\epsilon_r} \right) \cdot E_0 f\left(t - \frac{l}{c}\right), \quad (9)$$

$$= h_{eff2} E_0 f\left(t - \frac{l}{c}\right), \quad t < (k+1) \frac{l\sqrt{\epsilon_e} - l}{c}$$

$$h_{eff1} = \frac{h}{2}, \quad (10)$$

$$h_{eff2} = \frac{h}{2} \left(\frac{1 - \frac{1}{\epsilon_r}}{\sqrt{\epsilon_e} - 1} - \frac{1}{\epsilon_r} \right). \quad (11)$$

Where h_{eff1} and h_{eff2} are the theoretical effective heights, which are mainly determined by h . From (8) and (9), the amplitude E_0 and the waveform f of the incident electric field can be calculated respectively.

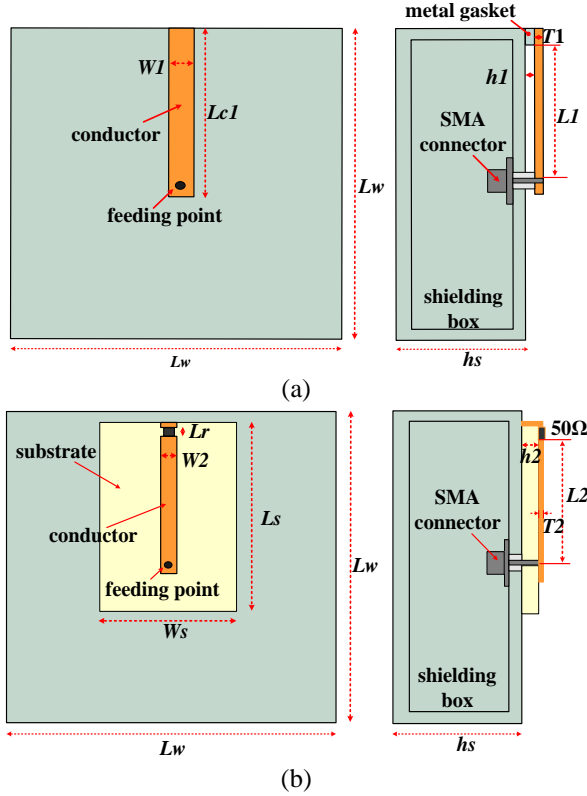


Fig. 2. Geometry of microstrip structures (the left is top view; the right is side view): (a) microstrip structure 1, and (b) microstrip structure 2.

C. The geometry of microstrip structures

The geometry of the microstrip structure without the substrate is shown as Fig. 2 (a). A shielding box occupying a size of $100 \times 100 \times 30$ mm³, which is equivalent to the ground plane of the microstrip line, is used to hold electro-optical conversion circuits. At the start of the microstrip structure, the conductor is connected to the top surface of the shielding box through a metal gasket with a size of $4.3 \times 4 \times 1$ mm³ for short circuit ($Z_1=0$). The end of the microstrip structure is connected to a 50 Ω SMA connector for the transmission of the induced voltage $U_{without_sub}$. The effective length $L1$ of the conductor is 45 mm, corresponding to a delay time t_0 of 0.3 ns. The geometry of microstrip structure 2 with a substrate is shown in Fig. 2 (b). The substrate is a microwave composite substrate with relative permittivity $\epsilon_r = 9.8$ and loss tangent $\sigma < 0.001$ and is equipped on the upper surface of the shielding box. A 50 Ω resistor is loaded at the start of the microstrip structure to match it with the microstrip structure. Similarly, a 50 Ω SMA

connector is connected to the end of the conductor to output the induced voltage U_{with_sub} . Both of the feeding positions of microstrip structures are set on the middle point of the upper surface of the shielding boxes. The effective length $L2$ of the conductor is 43 mm, corresponding to a delay time t_0 of 0.225 ns.

The final dimensions of two microstrip structures are summarized in Table 1.

Table 1: Dimensions of microstrip structures

Parameter	Value (mm)	Parameter	Value (mm)
$L1$	45	$L2$	43
$h1$	1	$h2$	3.175
$T1$	1	$T2$	0.035
$W1$	4.2	$W2$	3
$Lc1$	52	Lr	1
hs	30	Ls	60
Lw	100	Ws	40

III. PERFORMANCE SIMULATION

A. The recovered waveforms of two microstrip structures

The performances of the microstrip structures are studied by the Microwave CST studio based on the time-domain finite integration technique [15]. To study the performance of the microstrip structures, a simulation model of mono-cone structure which can generate UWB-SP is built, as shown in Fig. 3.

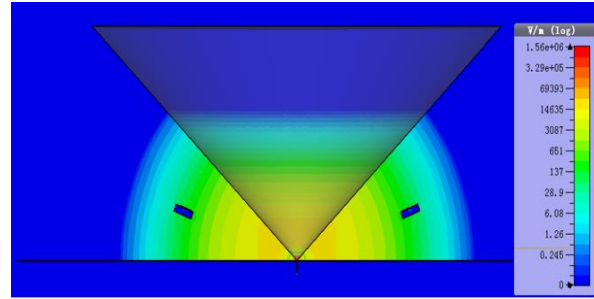


Fig. 3. Microstrip structure 1 (the right) and microstrip structure 2 (the left) activated by the electric field generated by the mono-cone structure.

The mono-cone structure is a variation of the infinite biconical transmission line, which contains a cone with half cone-apex angle of $\theta_h = 47^\circ$ and generatrix length of 1.5 m, a ground plane with a size 3×3 m. The dominant mode in the biconical line is the spherical TEM mode. Both of the microstrip structures are placed on the working area of the mono-cone structure symmetrically, where $r = 0.65$ m, $\theta = 21^\circ$. At this position, there is a clear time or time window of about 6 ns. Within the time window, the reflections from the ends of the cone and the

ground plane cannot affect the electromagnetic field of this position. Otherwise, the end reflections cannot be neglected.

A bipolar pulse with the rise time of 1 ns and the peak-to-peak width of 1.4 ns is set as the excitation signal and is sent into the mono-cone structure by a coaxial line under the ground plane. In order to monitor the output voltages, two voltage probes are set between the inner conductor and the outer conductor of coaxial lines connected to the SMA connectors in the shielding boxes, where the ends of the coaxial lines are matched with waveguide ports. According to (8) and (9), the recovered waveforms of two microstrip structures can be calculated, respectively. Figure 4 shows the comparison between the excited waveform and the recovered waveforms of two microstrip structures.

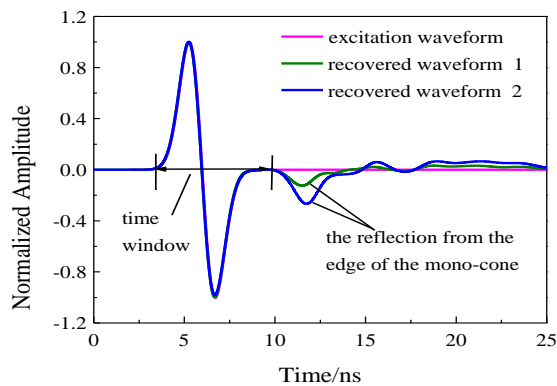


Fig. 4. The comparison between the recovered waveforms and the excited waveform.

As illustrated in Fig. 4, the recovered waveforms are highly consistent with the incident waveform within the time window of the mono-cone structure. The waveforms after the time of 10 ns are from the reflection of the edge of the mono-cone structure. The result reveals that the method of recovering the incident electric field mentioned above is effective and can be used to recover the waveform of the transient electromagnetic pulse.

B. Bandwidths of microstrip structures

From (8), (9), and (2), under the conditions that the feeding positions are well matched, the start is well short circuited for microstrip structure 1, and the start is well matched for microstrip structure 2, the amplitude responses are flat and the phase responses are linear. Thus, the incident electric fields will be recovered without distortion.

Actually, with the increase of the working frequency, the parasitic inductance and the parasitic capacitance of both ends of microstrip structure cannot be ignored, destroying the conditions. So, instead of the incident electric field formed by the mono-cone

structure, a signal peak pulse with the upper frequency limit of 2.5 GHz is adopted as the excitation signal. Fourier transform is used to calculate the spectrums of the excited signal and the recovered voltage. Then, the transfer functions of two microstrip structures can be calculated. The results are shown in Fig. 5.

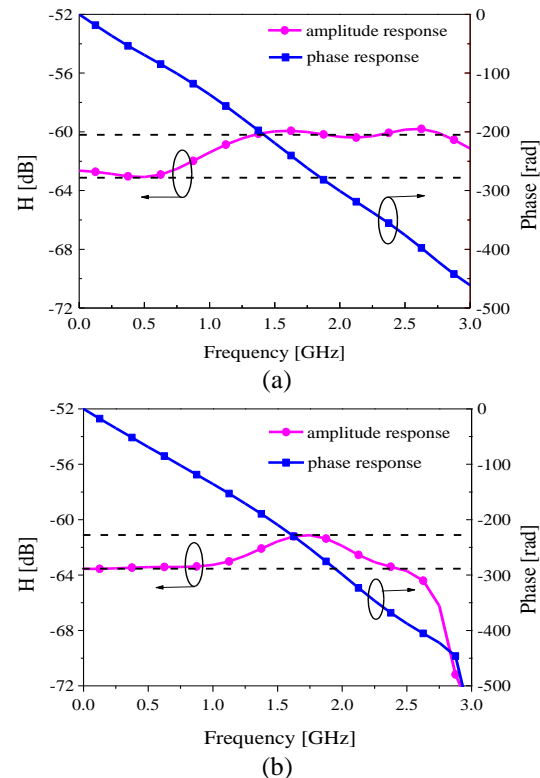


Fig. 5. Transfer functions of two microstrip structures: (a) microstrip structure 1, and (b) microstrip structure 2.

It can be seen from Fig. 5 that the bandwidth of -3 dB is DC~1.5 GHz for microstrip structure 1, and DC~2.5 GHz for microstrip structure 2. In these ranges, the amplitude response is approximately flat and the phase response is approximately straight line, satisfying the distortionless condition mentioned above approximately. The results signify that the microstrip structures have wide bandwidth for the measurement of transient electric field.

C. Effective heights of microstrip structures

Assuming that the recovered voltage is $U(t)$, and the excited electric field is $E(t)$, the effective height h_{eff} of microstrip structure defined as the ratio of $U(t)$ and $E(t)$ can be calculated. A signal peak pulse with the spectrum from DC to 1.5 GHz is used as the excited signal. The simulated and theoretical h_{eff} (h_{eff1} and h_{eff2}) are listed in Table 2. The simulated values are larger than the theoretical values. The reason is that the theoretical

analysis does not consider the effect of the height of the shielding box and the thickness of the conductor.

Table 2: Effective heights of microstrip structures

Microstrip Structures	Simulated h_{eff} (mm)	Theoretical h_{eff} (mm)
1	0.67	0.50
2	0.81	0.75

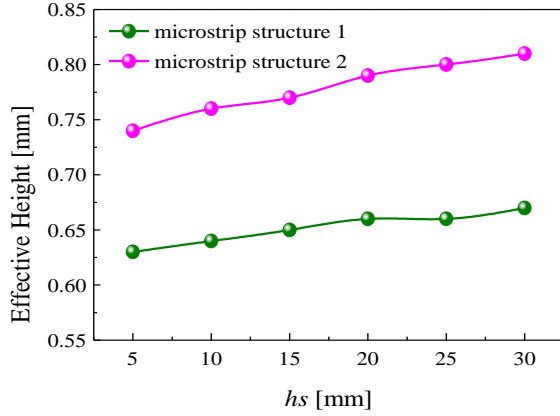


Fig. 6. The influence of height of shielding box on the effective height.

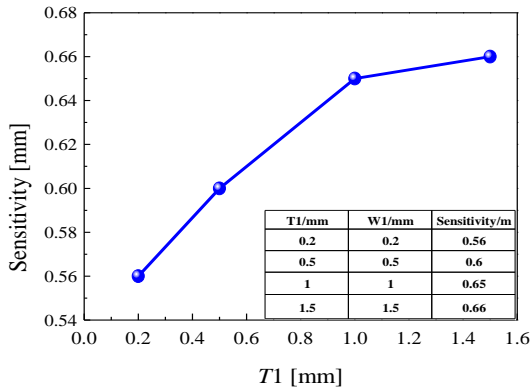


Fig. 7. The influence of the dimension of the conductor on the effective height.

Figure 6 presents the effective heights of microstrip structures with different h_s of shielding box. Figure 7 shows the influence from the dimension of the conductor of microstrip structure 1 on the effective height. It is clear that the thickness of the conductor is thinner, and the height of the shielding box is lower, the simulated effective height is closer to the theoretical effective height.

IV. EXPERIMENTAL VERIFICATION

A. Calibration of the microstrip structures

To verify the simulation results, the proposed

microstrip structures, as shown in Fig. 8, have been fabricated and tested by the time-domain electromagnetic pulse standard field generation setup [16].

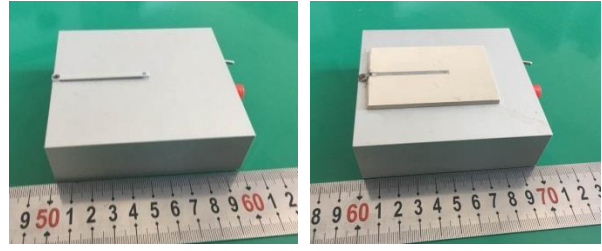


Fig. 8. The photos of microstrip structures. (Microstrip sensors can be built by adding the electro-optical conversion modules into the shielding boxes): (a) microstrip structure 1, and (b) microstrip structure 2.

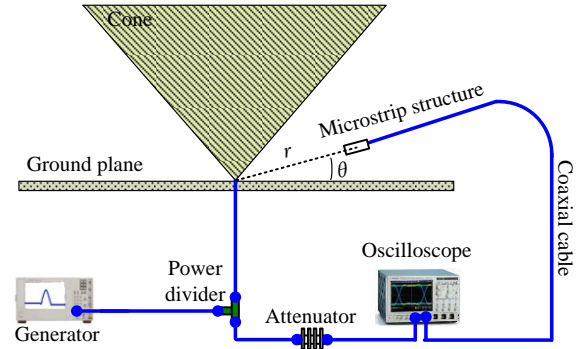


Fig. 9. Experiment system.

The experiment system is built up as shown in Fig. 9. The standard field generation setup is based on a monocone. It can produce a calculated electric field that only depends on the geometry parameter and the generator. Microstrip structure 1 is positioned on the working area of $r = 0.65$ m, $\theta = 21^\circ$ with a time window of about 6 ns, while microstrip structure 2 is positioned on the working area of $r = 0.8$ m, $\theta = 21^\circ$ with a time window of about 5 ns. A double peak pulse with the rise time of 1 ns and the peak-to-peak width of 2 ns, whose frequency spectrum is covered by the simulated bandwidth of the microstrip structures, is used as the excited signal. The output signals of microstrip structures are transmitted to channel 2 of the oscilloscope via a coaxial cable. Channel 1 of the oscilloscope can be used to monitor the incident electric field of the working area as the reference signal. To quantify the comparison between the recovered signal $U(t)$ from the output signal and the reference signal $V(t)$. The root mean square deviation σ is used [17]:

$$\sigma = \sqrt{\int_T [u(t-t_0) - v(t)]^2 dt / \int_T v^2(t) dt}, \quad (12)$$

where,

$$u(t) = U(t) / \sqrt{\int_T U^2(\tau) d\tau}, \quad (13)$$

$$v(t) = V(t) / \sqrt{\int_T V^2(\tau) d\tau}, \quad (14)$$

are normalized functions, T is the time window, and t_0 is the time shift of $V(t)$ relative to $U(t)$ wherein the value of σ is minimal.

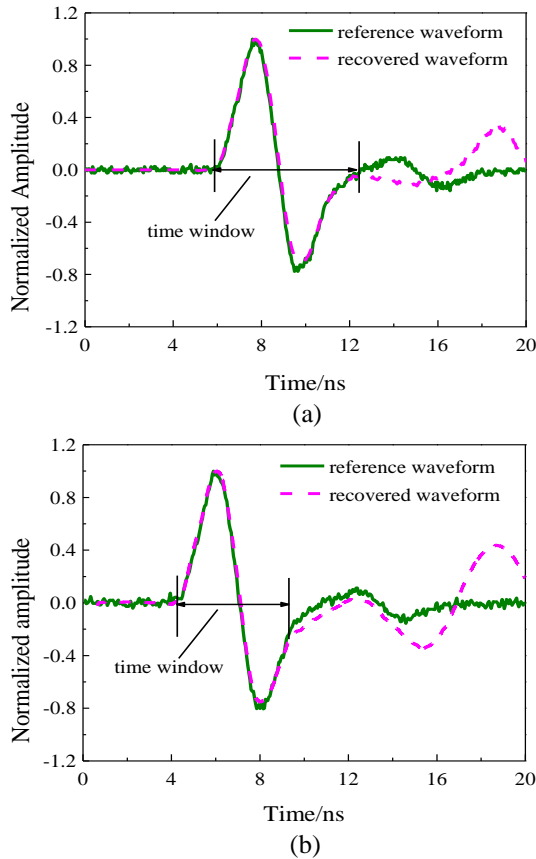


Fig. 10. The comparison of waveforms between the reference waveform and the recovered waveform: (a) microstrip structure 1, and (b) microstrip structure 2.

Figure 10 shows a comparison of waveforms between the reference waveform and the recovered waveform. As shown in Fig. 10, within the time window, the recovered waveforms from both microstrip structure 1 and microstrip structure 2 are highly similar to the corresponding reference waveforms. For the waveforms of structure 1, the RMS deviation σ is 6.9%. For the waveforms of microstrip structure 2, the RMS deviation σ is 5.8%. The waveforms outside the time window are mainly from the reflections at the edge of the monocone. The measured results show that the microstrip structures have good waveform fidelity.

The peak-to-peak values of the reference signal $V(t)$ and the recovered signal $U(t)$ are used to compute the effective height according to Eq. (15),

$$h_{eff} = \frac{U(t)r \sin(\pi/2 - \theta)}{1.2V(t)}. \quad (15)$$

For microstrip structure 1, the mean value of the effective height is 0.69 mm. The difference between the measured value and the simulated value is less than 3%. For microstrip structure 2, the mean value of the effective height is 0.78 mm, and the difference is less than 4%. The measured results show good consistency with the simulated results. The proposed microstrip structures can capture the transient electromagnetic field with the fast rise time of ≥ 1 ns.

B. Response of the microstrip sensors

According to the experimental results above, electro-optical conversion modules [18], whose lower cutoff frequency is lower than 1 kHz and the upper cutoff frequency is higher than 350 MHz, are added into the shielding boxes of the microstrip structures to build the microstrip sensors.

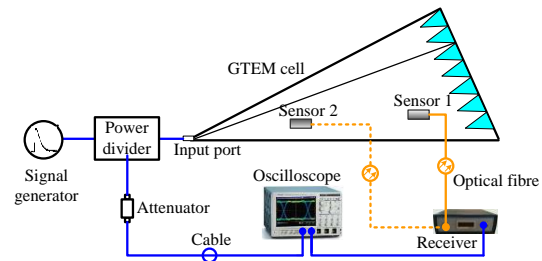


Fig. 11. Experiment test setup in GTEM cell.

As shown in Fig. 11, the GTEM cell [19] with $VSWR < 1.5$ GHz in the range of 1 KHz ~ 3 GHz, as the standard electro-magnetic field generating device, is used to test the response of the microstrip sensors. The signal generator is used to simulate the HEMP source and can generate a pulse with a rise time of 2 ns and a pulsewidth of 20 ns.

The output voltages of microstrip structures are converted into optical signals to transmit with a fibre and recorded by channel 2 of a digital oscilloscope, which can further improve the anti-interference ability for EMP during the transmission of signals. Channel 1 of the oscilloscope is used to monitor the source waveform. According to (8) and (9), the output signals are processed to get the recovered signals. The offset [20] from the noise of the electro-optical conversion circuit, the fibre and the oscilloscope are calculated and then compensated.

Figure 12 shows the comparison between the recovered waveforms and the source waveforms. It can be seen from Fig. 12 (a) that the recovered waveform from microstrip sensor 1 is basically consistent with the source waveforms. According to the IEEE Standard 1597.1 [21], the application of the feature selective validation techniques (FSV) gives for this comparison

the following values: GRADE = 2 and SPREAD = 2. The reason why the falling edge of the recovered waveform is different from that of the source waveform is from the reflection of the end of the GTEM cell. Microstrip sensor 2 is closer to the input port, which has a longer clear time than microstrip sensor 1. Figure 12 (b) illustrates that the recovered waveform is in agreement with the source waveform within the clear time. The RMS deviation σ is 5.3%. The FSV GRADE and SPREAD are 2 [22-23]. If the clear time is enough long, the falling edge of the source waveform can be recovered completely. These results indicate that the microstrip sensors can be used to measure HEMP.

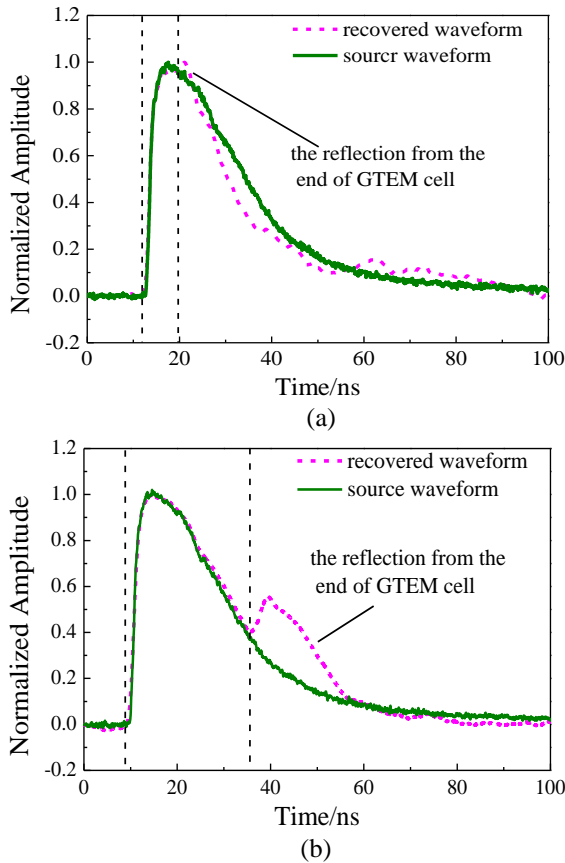


Fig. 12. The comparison between the recovered waveforms and the source waveforms: (a) microstrip structure 1 and (b) microstrip structure 2.

V. CONCLUSION

In order to detect the transient electric field, one type of microstrip structure and microstrip sensor is presented in this paper. The induced voltage on the end load of microstrip line is analyzed. The amplitude and the waveform of the incident electric field can be calculated from the induced voltage by the method of recovering the incident electric field. The proposed microstrip structures are set on the shielding boxes. The start of

microstrip structure 1 without substrate is short circuited, and the start of microstrip structure 2 with substrate is matched. The induced signals are outputted via the 50 Ω SMA connectors attached to the ends of the microstrip structures. The performances of two microstrip structures are simulated in the simulation model of a mono-cone structure and measured in the monocone. The simulated and the measured results confirm that the microstrip structures can capture the transient electromagnetic field with the fast rise time of ≥ 1 ns by the method mentioned above. In addition, the calibrated effective heights show consistency with the simulated effective heights. The reasons for the difference between the simulated effective heights and the theoretical effective height are analyzed. The simulated bandwidths of microstrip structure 1 and microstrip structure 2 are DC~1.5 GHz and DC~2.5 GHz, respectively. The measured results show that the microstrip sensors, built by adding the electro-optical conversion circuit into the shielding boxes, can measure HEMP, displaying its important role in the EMP effect and protection researches.

REFERENCES

- [1] C. E. Baum, "Reminiscences of high-power electromagnetics," *IEEE Transactions on Electromagnetic Compatibility*, vol. 49, no. 2, 2007.
- [2] IEC 6100-2-13, *High-Power Electromagnetic Environment—Radiated and Conducted*, 2005.
- [3] S. T. Song, "Simulation and analysis of HEMP coupling effect on a wire inside an apertured cylindrical shielding cavity," *ACES Journal*, vol. 27, no. 6, pp. 505-515, 2012.
- [4] W. A. Radasky, "Introduction to the special issue on high-power electromagnetics (HEMP) and intentional electromagnetic interference (IEMI)," *Electromagnetic Compatibility IEEE Transactions* vol. 46, no. 3, pp. 314-321, 2004.
- [5] X. Zhou, "Calculation of transient responses of EMP on transmission lines," *ACES-China 2017*, Suzhou, China, Aug. 2017.
- [6] J. R. Andrews, "UWB signal sources, antennas & propagation," *Wireless Communication Technology, 2003. IEEE Topical Conference on. IEEE*, pp. 439-440, 2003.
- [7] Electromagnetic Compatibility (EMC) – Part 2: Environment - Section 9: Description of HEMP environment - Radiated disturbance, International Electrotechnical Commission, IEC61000-2-9: 1996.
- [8] Y. S. Jiang, "Research on calibration accuracy of D-Dot transient electric field sensor," *Antenna Measurements & Applications (CAMA), 2017 IEEE Conference on. IEEE*, pp. 69-71, 2017.
- [9] W. Feser, "A potential free spherical sensor for the measurement of transient electric fields," *IEEE Transactions on Power Apparatus and Systems*, vol. PAS-103, no. 10, Oct. 1984.

- [10] Z. Cui, "E-field sensor design for subnanosecond fast transient," *Environmental Electromagnetics, 2012 6th Asia-Pacific Conference on. IEEE*, 2012.
- [11] S. V. Tikhomirov and K. Y. Sakharov, "A standard system for producing very-short electromagnetic pulses with a rise time of 20 psec," *Measurement Techniques*, vol. 53, no. 7, pp. 809-812, 2010.
- [12] K. Y. Sakharov, "A picosecond pulsed electric field strength measuring transducer," *Measurement Techniques*, vol. 57, no. 2, pp. 201-205, 2014.
- [13] K. Y. Sakharov, "A measuring system for characterization of radar-absorbing materials with sounding ultra-short electromagnetic pulses over the range 0.1-40 GHz," *Microwave Techniques (COMITE), 2015 Conference on. IEEE*, 2015.
- [14] S. A. Podosenov and A. A. Sokolov, "Linear two-wire transmission line coupling to an external electromagnetic field. I. Theory," *IEEE Transactions on Electromagnetic Compatibility*, vol. 37, no. 4, pp. 559-566, 1995.
- [15] CST STUDIO SUITE™ 2014, CST AG, Germany, www.cst.com, 2014.
- [16] Y. Yan, "Study of the time-domain electromagnetic pulse standard field generation setup and its application," *Review of Scientific Instruments*, vol. 89, no. 7, 2018.
- [17] E. V. Balzovsky, "Dual polarized receiving steering antenna array for measurement of ultra-wideband pulse polarization structure," *Review of Scientific Instruments*, vol. 89, no. 3, 2016.
- [18] J. Wei, "Development of transient electric field sensor based on microstrip line," *Microwave and Millimeter Wave Technology (ICMMT), 2018 IEEE International Conference on. IEEE*, Chengdu, China, May 2018.
- [19] Electromagnetic compatibility (EMC) – Part 4-20: Testing and measurement techniques – Emission and immunity testing in transverse electromagnetic (TEM) waveguides, IEC61000-4-20: 2010.
- [20] L. Yao, "Implementation of a measurement system on field uniformity of transient electromagnetic field," *IEEE Electromagnetic Compatibility Magazine*, vol. 5, no. 1, pp. 43-49, 2016.
- [21] IEEE, Standard for Validation of Computational Electromagnetics Computer Modeling and Simulations, Standard IEEE 1597.1-2008, June 2008.
- [22] A. Orlandi, G. Antonini, C. Ritota, and A. P. Duffy, "Enhancing feature selective validation (FSV) interpretation of EMC/SI results with grade-spread," in *Proc. 2006 IEEE Int. Symp. Electromagn. Compat.*, vol. 2, pp. 362-367, 2006.
- [23] A. P. Duffy and A. Orlandi, "The influence of data

density on the consistency of performance of the feature selective validation (FSV) technique," *J. Appl. Comput. Electromagn. Soc.*, vol. 21, no. 2, pp. 164-172, 2006.



Jinhong Wei was born in 1991 in Yunnan, China. He received his B.Sc. degree from Xi'an Jiaotong University, Xi'an, China, 2014, and the M.S. degree from Northwest Institute of Nuclear Technology, Xi'an, China, in 2016. He has been an Engineer in Northwest Institute of Nuclear Technology, Xi'an, China. His current research interests include the transient electromagnetic measurement and antenna design.



Shoulong Zhang received the M.S. degree from Army Engineering University, Shijia-zhuang, China, in 2014. He has been an Engineer in Northwest Institute of Nuclear Technology, Xi'an, China. His current research interests include EMP measurement and RF circuit design.



Zhen Liu received his B.Sc. degree in Electronics Engineering and Computer Science from Peking University, Beijing, China, 2010, and the M.S. degree from National University of Defense Technology, Changsha, China, in 2012. He has been an Engineer in Northwest Institute of Nuclear Technology, Xi'an, China. His current research interests include time-domain electromagnetics and its applications.



Youjie Yan received the Ph.D. degree at the University of Electronic Science and Technology of China, Chengdu, China, in 2018. He has been an Associate Research Fellow in Northwest Institute of Nuclear Technology, Xi'an, China. His research interests include the time-domain electromagnetics and the electromagnetic compatibility.



compatibility.

Tingyong Jiang received the Ph.D. degree from Tsinghua University, Beijing, China, in 2016. He has been a Senior Engineer in the Northwest Institute of Nuclear Technology, Xi'an, China. His current research interests include time-domain electromagnetics and the electromagnetic



interests include time-domain electromagnetics and its applications.

Fanghong Huang received the M.S. degree in Measurement Techniques and Instruments from National University of Defense Technology, Changsha, China, in 2016. She has been an Engineer in the Northwest Institute of Nuclear Technology, Xi'an, China. Her current research